Experimental Neurology 333 (2020) 113430

Contents lists available at ScienceDirect

Experimental Neurology

journal homepage: www.elsevier.com/locate/yexnr

Research paper

Neuronal mitochondrial calcium uniporter deficiency exacerbates axonal injury and suppresses remyelination in mice subjected to experimental autoimmune encephalomyelitis

Scott P. Holman[a,b], Aurelio S. Lobo[a,b], Robyn J. Novorolsky[a,b], Matthew Nichols[a,b], Maximillian D.J. Fiander[a,b], Prathyusha Konda[c], Barry E. Kennedy[c], Shashi Gujar[c], George S. Robertson[a,b,d,*]

[a] Department of Pharmacology, Brain Repair Centre, Dalhousie University, 1348 Summer Street, Life Sciences Research Institute, North Tower, Halifax B3H 4R2, Canada
[b] Faculty of Medicine, Dalhousie University, 1348 Summer Street, Life Sciences Research Institute, North Tower, Halifax B3H 4R2, Canada
[c] Department of Pathology, Faculty of Medicine, Dalhousie University, 1348 Summer Street, Life Sciences Research Institute, North Tower, Halifax B3H 4R2, Canada
[d] Department of Psychiatry, 5909 Veterans' Memorial Lane, 8th Floor, Abbie J. Lane Memorial Building, QEII Health Sciences Centre, Halifax B3H 2E2, Canada

ARTICLE INFO

Keywords:
Autophagy
Calpain activation
Demyelination
Mitochondrial calcium uptake
Multiple sclerosis

ABSTRACT

High-capacity mitochondrial calcium (Ca^{2+}) uptake by the mitochondrial Ca^{2+} uniporter (MCU) is strategically positioned to support the survival and remyelination of axons in multiple sclerosis (MS) by undocking mitochondria, buffering Ca^{2+} and elevating adenosine triphosphate (ATP) synthesis at metabolically stressed sites. Respiratory chain deficits in MS are proposed to metabolically compromise axon survival and remyelination by suppressing MCU activity. In support of this hypothesis, clinical scores, mitochondrial dysfunction, myelin loss, axon damage and inflammation were elevated while remyelination was blocked in neuronal MCU deficient (Thy1-MCU Def) mice relative to Thy1 controls subjected to experimental autoimmune encephalomyelitis (EAE). At the first sign of walking deficits, mitochondria in EAE/Thy1 axons showed signs of activation. By contrast, cytoskeletal damage, fragmented mitochondria and large autophagosomes were seen in EAE/Thy1-MCU Def axons. As EAE severity increased, EAE/Thy1 axons were filled with massively swollen mitochondria with damaged cristae while EAE/Thy1-MCU Def axons were riddled with late autophagosomes. ATP concentrations and mitochondrial gene expression were suppressed while calpain activity, autophagy-related gene mRNA levels and autophagosome marker (LC3) co-localization in Thy1-expressing neurons were elevated in the spinal cords of EAE/Thy1-MCU Def compared to EAE/Thy1 mice. These findings suggest that MCU inhibition contributes to axonal damage that drives MS progression.

1. Introduction

MS is characterized by the autoimmune-mediated destruction of myelin that insulates axons in the central nervous system (CNS) (Charcot, 1868; Compston and Coles, 2008). Immune-targeting therapies reduce disease relapses but have limited value in halting the neurodegenerative processes responsible for MS disease progression (Dendrou et al., 2015; Kapoor et al., 2018; Kappos et al., 1998; Lublin et al., 2016; Montalban et al., 2017). Convergent evidence from genetic association, transcriptional profiling, proteomic, biochemical and imaging studies implicate a host of mitochondrial deficits including impaired respiration, Ca^{2+} buffering, motility, undocking and integrity in the unrelenting loss of CNS axons that mark MS disease progression (Campbell and Mahad, 2018; Campbell and Mahad, 2012; Dutta et al., 2006; Franklin et al., 2012; Trapp et al., 1998; Witte et al., 2014; Witte et al., 2013). However, the precise mechanisms are unclear (Peruzzotti-Jametti and Pluchino, 2018). To be relevant for progressive MS, we propose that disease models should reproduce these features of mitochondrial dysfunction in a manner that closely precedes CNS axon injury. In addition to improving our understanding of how mitochondrial dysfunction promotes MS progression by damaging axons and disrupting remyelination, such models would also assist the development of more effective treatments.

Mitochondrial Ca^{2+} uptake, driven by the mitochondrial membrane

* Corresponding author at: Brain Repair Centre, Faculty of Medicine, Dalhousie University, 1348 Summer Street, Life Sciences Research Institute, North Tower, Halifax B3H 4R2, Canada.
E-mail address: robertgs@dal.ca (G.S. Robertson).

https://doi.org/10.1016/j.expneurol.2020.113430
Received 19 May 2020; Received in revised form 5 July 2020; Accepted 28 July 2020
Available online 01 August 2020

potential (Ψ_m), was clearly demonstrated in 1961 (Deluca and Engstrom, 1961). Genetic identification of the mitochondrial Ca^{2+} uniporter (MCU) in 2011 revealed that high-capacity mitochondrial Ca^{2+} uptake is mediated by the MCU (Baughman et al., 2011; De et al., 2011). This has allowed the generation of conditional MCU deficient murine lines for which MCU activity in cardiac myocytes or CNS neurons is suppressed by tamoxifen-induced *cre* recombination at floxed sites critical for MCU function. These inducible knockout lines have shown that the MCU regulates both cell death and survival. With respect to the former, excessive MCU activity triggers mitochondrial Ca^{2+} overloading resulting in ischemic/reperfusion heart and brain injury (Kwong et al., 2015; Luongo et al., 2015; Nichols et al., 2018). In the case of the latter, enhanced entry of Ca^{2+} into the matrix *via* the MCU increases ATP synthesis by allosterically activating dehydrogenases that produce reducing equivalents which fuel complex I activity (Denton et al., 1972; Nichols et al., 2017; Rizzuto et al., 2012). MCU-mediated mitochondrial Ca^{2+} uptake may also promote neuronal survival by buffering intracellular Ca^{2+} concentrations that oppose injurious Ca^{2+}-dependent phospholipase and protease activities (Stirling and Stys, 2010; Trapp and Stys, 2009). In response to the dynamic energy demands imposed by neurotransmission, mitochondria are rapidly transported along the axon by cytoskeletal motors to metabolically active sites (Saxton and Hollenbeck, 2012; Schwarz, 2013). Increased MCU-mediated Ca^{2+} uptake, triggered by elevated Ca^{2+} concentrations at these active sites, undocks mitochondria from their cytoskeletal motors (Chang et al., 2011; Niescier et al., 2013; Niescier et al., 2018). This positions mitochondria at metabolically active neuronal sites in urgent need of increased Ca^{2+} buffering and ATP synthesis.

Demyelination places a considerable metabolic burden on axons that must produce massive amounts of ATP to support increased ion pumping by sodium/potassium adenosine triphosphatase (Stys and Lopachin, 1998; Trapp and Stys, 2009; Tsutsui and Stys, 2013). Increased MCU activity may thus be required to meet the prodigious metabolic demands imposed by demyelination on axons. Oxidative phosphorylation generates the Ψ_m by pumping hydrogen ions into the intermembrane space (Lehninger, 1979). ATP synthase harvests this proton gradient to produce ATP (Hahn et al., 2018). Respiratory deficits seen in progressive MS axons (Campbell and Mahad, 2012; Dutta and Trapp, 2012; Fischer et al., 2012; Mahad et al., 2009; Witte et al., 2014) would thus suppress ATP synthesis by depolarizing the Ψ_m. Since the Ψ_m drives mitochondrial Ca^{2+} uptake (Rottenberg and Scarpa, 1974), we propose that respiratory deficits in progressive MS reduce axonal MCU activity. Confocal imaging has shown that depolarization of the Ψ_m in spinal cord axons is also associated with increased disease severity while recovery was accompanied by repolarization of the Ψ_m (Sadeghian et al., 2016). These findings indicate that autoimmune-mediated demyelination places a massive metabolic stress on spinal cord axons that impairs the movement of EAE mice.

In view of the potential for impaired axonal MCU activity to promote MS disease progression, we have examined the effects of inducible MCU deletion in Thy1-expressing neurons of mice subjected to EAE. Clinical scores, myelin loss, axonal injury, ATP concentrations, mitochondrial gene expression, calpain activity, immune cell infiltration, cytokine expression and autophagy markers were compared in the spinal cords of these EAE/Thy1-MCU Def mice and EAE/Thy1 controls with intact MCU function. Morphologies indicative of mitochondrial activation, swelling and fragmentation, cytoskeletal loss, autophagosome formation and axonal damage and remyelination were also quantified in electron microscopic images of axons located within L5 of the spinal cord at different stages of disease development in EAE/Thy1 and EAE/Thy1-MCU Def mice.

2. Materials and methods

2.1. Animal care

Experimentation was approved by the Dalhousie University Committee on Laboratory Animals in accordance with the Canadian Council on Animal Care and ARRIVE Guidelines. Animal holding rooms were on a 12-h dark/light cycle. Water and food were provided *ad libitum*.

2.2. Generation of cortical-neuron specific MCU deficient mice

Single-neuron Labelling with Inducible Cre-mediated Knockout-H (SLICK-H; The Jackson Laboratory; Stock No: 012708) mice expressing a Thy1-cre/ERT2-eYFP construct were crossed with C57BL/6 MCU-floxed ($MCU^{fl/fl}$) mice (Dr. Jeffrey Molkentin, Philadelphia, Ohio, USA) to generate Thy1-cre/ERT2-$eYFP^{+/-}$/$MCU^{fl/fl}$ mice. These mice were given tamoxifen (TMX; 80 mg/kg) once daily for 5 days by oral gavage followed by a 3-week washout period to ablate the MCU in Thy1-expressing neurons (Thy1-MCU Def mice). SLICK-H mice treated in the same manner served as controls (Thy1 mice).

2.3. Induction of EAE

Female mice were used for all experimentation at 12 weeks of age. Thy1 and Thy1-MCU Def mice were immunized by subcutaneous injection of 300 μg of myelin oligodendrocyte glycoprotein 35–55 ($MOG_{35–55}$; GenScript, Piscataway, NJ, USA) emulsified in Complete Freund's Adjuvant (CFA) on day post immunization (DPI) 0. Pertussis toxin (PTX; Sigma, St. Louis, MO, USA) was injected intraperitoneally (300 ng/mouse) on DPI 0 and 2. Thy1 and Thy1-MCU Def mice that received CFA emulsified with PBS instead of $MOG_{35–55}$ (200 μl/mouse) followed by PTX on DPI 0 and 2 served as $MOG_{35–55}$ immunization controls (CFA groups). If weight loss exceeded 10%, mice received ip injections of saline to prevent dehydration and mashed food chow that prevented animal mortality.

2.4. Behavioural assessment of clinical scores

The following ordinal scale was used to clinically score the animals for degree of motor deficit: 0, no clinical signs; 0.5, hooked tail; 1, flaccid tail; 1.5, flaccid tail with splay; 2, minor walking deficits, mild ataxia; 2.5, severe walking deficits; 3, dropped pelvis in addition to severe walking deficits, chronic ataxia; 3.5, unilateral hindlimb paralysis; 4, bilateral hindlimb paralysis; 4.5, forelimb paralysis; 5, moribund. A trained observer who was blinded to the treatment conditions recorded all clinical scores starting at DPI 7.

2.5. Preparation of spinal cord tissue for histology

Mice were euthanized at DPI 16 or 30 with an overdose of sodium pentobarbital (150 mg/kg, ip; Schering Canada Pointe-Claire, Quebec) and perfused with PBS (10 ml) followed by 4% paraformaldehyde (PFA, 10 ml; Fisher Scientific, Fair Lawn, New Jersey, USA). Spinal cords were isolated from the spinal column by microdissection, post-fixed in 4% PFA for 24 h and placed in 15% sucrose (24 h) followed by 30% sucrose (24 h) for cryoprotection. The spinal cords were then trimmed to a segment spanning lumbar vertebrae 2–5 (L2–5) and allocated for sectioning in either the coronal or sagittal planes. L2–5 spinal cord segments were embedded vertically or horizontal in Tissue-Tek® optimal cutting temperature (OCT; Sakura® Finetek, USA). Serial sagittal sections (30 μm thick) were then cut at −18 °C with a cryostat (Leica CM1950).

2.6. Eriochrome cyanine (ER) staining and immunohistochemistry

Spinal cord sections at DPI 16 and 30 were rehydrated with descending concentrations of ethanol (100% to 70%) before being dipped in tap water. Sections were then stained with ER (Sigma Aldrich) for 15 min, differentiated in 0.5% ammonium hydroxide solution and rinsed in tap water. Sections were counterstained with neutral red (Acros Organics) for 2 min and rinsed once more with tap water. Sections were then dehydrated in ascending concentrations of ethanol (70%–100%), washed in xylene and cover-slipped with Cytoseal 60 (Thermo Scientific). Immunohistochemistry was also performed on longitudinal spinal cord sections from DPI 16 mice. Sections were blocked for 1 h at room temperature with 20% normal goat serum in PBS/0.5% Triton X-100. Slides were then incubated overnight in rabbit anti-LC3b (L7543, 1:400, Sigma-Aldrich, St. Louis, Missouri, USA) at 4 °C. Slides were then washed 3 times with PBS and incubated with goat anti-rabbit alexafluor 647 (ab150079, 1:250, Abcam, Cambridge, UK) at 23 °C for 1 h. Slides were then coverslipped with Fluoromount (Sigma Aldrich, St. Louis, MO, USA) and eYFP and LC3 fluorescence was visualized using a Zeiss Axio Imager Z2 with monochrome camera (Zeiss, Pleasanton, CA, USA).

2.7. Western blotting

Spinal cords from CFA/Thy1, EAE/Thy1, CFA/Thy1-MCU Def and EAE/Thy1-MCU Def mice euthanized at DPI 16 were homogenized in 500 μl RIPA buffer including a protease inhibitor cocktail (Sigma-Aldrich, Oakville, ON, Canada) and then spun at 14,000 *g* for 15 min at 4 °C. The supernatant was collected into fresh microtubes and the protein concentration determined by Bradford assay (Bio-Rad Laboratories Inc., Mississauga, ON, Canada). After thawing, 10 μg protein samples were electrophoretically separated on 10% sodium dodecyl sulfate polyacrylamide gels and transferred onto Amersham Hybond 0.2 μm PVDF membranes (GE Healthcare Life sciences, Germany) at 220 mA for 2 h. The protein containing PVDF membranes were then blocked in 5% non-fat milk (Santa Cruz Biotechnology, Dallas, TX, USA) for 1 h and washed 3× in Tris-base Saline with 0.05% Tween-20. The membranes were incubated overnight at 4 °C in primary antibodies prepared in 1% non-fat milk and at dilutions according to manufacturer's instructions. The antibodies utilized included: rabbit anti-MCU D2Z3B (149,975, Cell Signaling Technology, Danvers, MA, USA), mouse anti-β-actin antibody (055 K4854, Sigma, St. Louis, Missouri, USA), rabbit anti-β-tubulin (ab6046, Abcam, Cambridge, UK) and mouse anti-α-Fodrin (AA6; BML-FG6090–0100, Enzo Life Sciences, Inc., Cedarlane, Burlington, ON, Canada). Blots were incubated with peroxidase-labelled goat anti-rabbit IgG PI-1000 or goat anti-mouse IgG PI-2000 (Vector Laboratories, Burlingame, CA, USA) for 1 h and washed. Amersham ECL prime western blotting detection reagent (GE Healthcare Life Sciences, Germany) was applied to the membrane immediately before imaging. Images were captured with a ChemiDoc Touch and analysed with Image Lab 6.0 software (Bio-Rad Laboratories, Inc., Mississauga, ON, Canada). MCU levels are shown as the ratio relative to the β-tubulin signal. Calpain activation reflected the optical density ratio of calpain-cleaved fragment of αII-spectrin (150 kDa) divided by intact αII-spectrin (285 kDa).

2.8. Transmission electron microscopy (EM)

Spinal cords were fixed in 2.5% glutaraldehyde by perfusion in PBS (pH 7.4). The samples were then rinsed 3 times in 0.1 M sodium cacodylate buffer and fixed in 1% osmium tetroxide for 2 h and, after dehydration, embedded in epon araldite resin. Sections 100 nm thick were cut with an ultramicrotome and placed on mesh copper grids which were stained with 2% aqueous uranyl acetate, rinsed, and treated with lead citrate, then rinsed again and air dried. Images were captured with a Jeol Jem 1230 transmission electron microscope at 80 kV equipped with a Hamatsu ORCA-HR digital camera. Mitochondria (activated, condensed/fragmented or swollen) per axon, autophagosomes per axon, damaged axons, remyelinating axons and mitochondria per remyelinating axon were manually counted within an area (10 × 10 μm) in the L5spinal cord. Four regions within ten serial sections images, selected at random, were quantified for each of the EAE/Thy1 (n = 20) and EAE/Thy1-MCU Def (n = 20) mice with CS = 0, 2.0, 2.5, 3.0 or 3.5 (n = 4/CS). Optical densities were also measured within an area (2 × 2 μm) located within L5 spinal cord axons of EAE/Thy1 and EAE/Thy1-MCU Def mice at CS = 2.0 using image J software. The average values for measurements made by two individuals blinded to the experimental conditions were used for the statistical comparisons.

2.9. Cell preparation for flow cytometry

Spleens were harvested aseptically at DPI 16 and kept in chilled sterile Ca^{2+} and Mg^{2+} free PBS (Gibco; Life technologies, Grand Island, NY, USA) on ice. Individual spleens were filtered through a 40 μm Nylon cell strainer (BD Falcon, Bedford, MA, USA) in a 50 ml conical tube. The crushed cells were filtered, washed with 5 ml PBS and centrifuged at 500 rpm for 10 min at 4 °C. The supernatant was aspirated and discarded while the pellet was resuspended in 4 ml/spleen of 1× sterile ACK lysis buffer and allowed to stand at room temperature for 15 min. The lysis buffer was then neutralized with 6 ml of sterile complete RPMI medium (Gibco; Life technologies, Grand Island, NY, USA) which contained 1% heat inactivated fetal bovine serum (FBS, Mediatech, Inc., Corning subsidiary, Manassas, VA, USA). The neutralized cell suspension was then passed through a 40 μm Nylon cell strainer to exclude any cell clumps and was centrifuged at 500 rpm for 10 min at 4 °C. The supernatant was discarded, and cells resuspended in complete RPMI medium at 10 × 10^6 cells per ml before FACS analysis. Mice were perfused with ice-cold 1× Hank's Balanced Salt Solution (HBSS, Gibco by Life Technologies, Grand Island, NY, USA) without Ca^{2+} and Mg^{2+}. CNS tissue was dissected and maintained in RPMI without phenol red (Gibco by Life Technologies, Grand Island, NY, USA) until all the mice were sacrificed. CNS tissue from individual mice was homogenized together in a Dounce homogenizer in RPMI and the cell suspension was then made up to 7 ml with RPMI. Stock isotonic percoll (SIP) was prepared by mixing 9 parts of percoll (MP Biomedicals, LLC, Santa Ana, CA, USA) with one part of 10× HBSS without Ca^{2+} and Mg^{2+}. The cell suspension was mixed with 3 ml SIP to get 30% SIP which was slowly overlayered on top of 2 ml of 70% SIP in 1× HBSS. The overlayered cells were centrifuged at 500 rpm for 30 min at 18 °C with minimal or no breaks so that the interface was not disturbed. Approximately 2–3 ml of the 70%–30% interphase was collected into a fresh tube and washed twice by resuspending the cells in 1× HBSS and centrifugated at 500 rpm for 7 min at 18 °C. The pellet was resuspended in complete RPMI medium.

2.10. Flow cytometry

For all experiments, approximately 1 × 10^6 cells were resuspended in FACS buffer (1% FBS in PBS with 5 mM EDTA). Centrifugation was carried out at 500 rpm for 5 min at 4 °C. Cells were incubated in purified anti-mouse CD16/CD32 (BD Biosciences, San Jose, CA, USA) in FACS buffer for 30 min at 4 °C to block the F_C binding sites. Surface staining was performed in the dark for 30 min at 4 °C in FACS buffer. Cells were then washed twice with FACS buffer and fixed in 4% paraformaldehyde (VWR, West Chester, PA, USA) for 20 min at room temperature. Cells were then washed twice, resuspended in FACS buffer, and stored at 4 °C until FACS analysis. Surface markers for these experiments include: anti-mouse CD4 antibody clone RM4–5 FITC (1:200, BioLegend); anti-mouse CD3ε antibody clone 145-2C11 PE (1:200, BioLegend); anti-mouse CD8a antibody clone 53–6.7 PerCP (1:200, BD Biosciences); anti-mouse Ly-6G antibody clone 1A8 FITC

(1:400, BD Biosciences); anti-mouse Ly-6C antibody clone HK1.4 PE (1:150, BioLegend); anti-mouse/human CD11b antibody clone M1/70 PerCP (1:400, BioLegend); anti-mouse CD45 antibody clone 30-F11 APC/Cy7 (1:200, BioLegend). The FACS experiments were performed using the FACS Canto II instrument (BD Immunocytometry systems, San Jose, CA, USA) equipped with 405 nm, 488 nm, 561 nm and 640 nm excitation lasers located in the Dalhousie University Faculty of Medicine Core Facility, Halifax, NS, Canada. All data collections were performed using the BD FACS Diva software (BD Biosciences, San Jose, CA, USA) and the data analyses were performed using Flowing software (Turku Centre for Biotechnology, University of Turku, Finland). Compensation was performed using single colour controls prepared for each fluorochrome on positive cell populations for the cell surface staining. Doublet discrimination was performed manually to exclude any composite events due to clumped cells.

2.11. Quantitative reverse transcription polymerase chain reaction (qRT-PCR)

Spinal cords harvested at DPI 16 were homogenized in 1 ml PureZOL (Bio-Rad Laboratories, Inc., Mississauga, ON, Canada) in the Benchmark Scientific D1030 homogenizer (Cole-Parmer Canada Company, Montreal, QC, Canada). Total RNA was extracted using the Aurum Total RNA Fatty and Fibrous Tissue kit (Bio-Rad Laboratories, Inc., Cat. #732–6870, Mississauga, ON, Canada) following the spin protocol as per the manufacturer's instructions. On elution, the concentration and purity of RNA was estimated spectrophotometrically on the SPECTROstar Nano spectrophotometer (BMG Labtech, Mandel Scientific Company Inc., Guelph, ON, Canada). To measure the quality and overall integrity of the isolated total RNA, the Experion bioanalyzer along with the RNA StdSens Analysis Kit (Bio-Rad Laboratories, Inc., Mississauga, ON, Canada) was used. Only samples with RNA Integrity Number (RIN) values of 7.5 or more were considered acceptable and used for further analysis. Reverse transcription was carried out with the iScript cDNA synthesis kit (Bio-Rad Laboratories, Inc., Mississauga, ON, Canada) using 1 μg of RNA as template for each sample. qRT-PCR was performed with the SsoFast EvaGreen Supermix kit (Bio-Rad Laboratories, Inc., Mississauga, ON, Canada) with β-actin, GAPDH, β2M and HPRT1 evaluated as reference genes (see attached Table). The individual genes were optimized for both annealing temperature and conditions. PCR cycling conditions were: (95 °C for 30 s) + (95 °C x 5 s + 60 °C x 5 s + fluorescence read) x 40 cycles + melt curve analysis. The melting curve program was a 2 s hold time with plate readings for every 0.5 °C increase from 65 °C to 95 °C. All qRT-PCR protocols were done in accordance with the MIQE guidelines (Bustin et al., 2009) and were performed with the Bio-Rad CFX96 real-time system C1000 touch thermal cycler (Bio-Rad Laboratories, Inc., Mississauga, ON, Canada). Data analysis was performed using the CFX Maestro software (Bio-Rad Laboratories, Inc., Mississauga, ON, Canada) using the $^{\Delta\Delta}$Cq method. Statistical comparisons were performed using the average value of triplicate technical replicates for all experiments. Primers used for qRT-PCR are shown in Supplementary Table 1.

2.12. Fluorometric calpain activity assay

Calpain activity was measured in the spinal cord at DPI 16 using a fluorometric calpain cleavage assay (K240–100; BioVision Inc., CA, USA) according to the manufacturer's protocol. Each well of a 96-well black plate was loaded with protein (50 μg) extracted from the spinal cord and reaction buffer. Active Calpain I (provided in the kit) was used as a positive control and treatment with the calpain inhibitor *Z*-LLY-FMK (provided in the kit) was used to confirm assay specificity. After incubation at 37 °C for 1 h in the dark, fluorescence was measured using a Synergy H1 hybrid multi-mode plate reader (BioTek Instruments, Inc., Vermont, USA).

2.13. ATP measurements in the spinal cord

Spinal cords harvested at DPI 16 were placed in ice-cold 2% trichloroacetic acid, homogenized for 1 min and neutralized with 10 mM Tris-acetate, 2 mM EDTA, pH 7.75. The homogenate was centrifuged at 13,000 rpm for 20 min at 4 °C and stored at −80 °C until analysis. The pellet obtained after centrifugation was washed twice in ice cold acetone and dried overnight at 37 °C in an oven. The dried pellet was reconstituted with 3 M Urea and protein estimation was carried out by Bradford assay. The ATP concentration was measured using the Invitrogen™ Molecular Probes™ ATP Determination Kit (Molecular Probes, Inc., Eugene, Oregon, USA). The pH of the samples was adjusted to 7.75 using Tris base pH = 10 immediately before ATP determination. The neutralized acid soluble supernatant (10 μl) or diluted ATP standard (10 μl) were added to 96-well microplates. The reaction was started by adding 90 μl of standard reaction solution to each well and luminescence read immediately using a FLUOstar Omega plate reader (BMG Labtech).

2.14. Power calculations

Power calculations were performed to determine the group sizes required to detect statistical differences at an alpha level of 0.05. A group size of 10 mice with a standard deviation (SD) of 45% was needed to detect a 50% difference between the means for clinical scores, myelin loss and axonal injury with 100% accuracy. Four mice/group with a SD of 25% detects a 65% difference between means for the EM measurements. Six mice/group with a SD of 30% was required to detect a 50% difference between the means for calpain activity, ATP concentrations and mitochondrial mRNA levels. Five mice/group with a SD of 25% was required to detect a 40% difference between the means for the cytometry measurements and counts for eYFP, LC3 and eYFP/LC3 positive cells in the spinal cord. Eight mice/group with an SD of 35% was needed to detect a 50% difference between the means for cytokines and atg mRNA levels.

2.15. Statistical analyses

A two-way analysis of variance (ANOVA) was used to compare clinical scores (CS) of EAE/Thy1 and EAE/Thy1-MCU Def mice (Fig. 1A). A one-way ANOVA followed by Tukey's multiple comparison tests were performed to assess potential differences between eYFP labelling in the corticospinal axons, myelin loss, calpain activation, ATP concentrations, SDH, mt-CO4, PGC-1α and atg mRNA levels, LC3 co-localization in eYFP positive spinal cord neurons, T lymphocyte and myeloid cell populations and cytokine mRNA levels (Fig. 1D; Fig. 2B; Fig. 2F-H; Fig. 6A-C; Fig. 7C-F; Fig. 8A-H). The Mann-Whitney *U* test was used to compare days at CS ≥ 1.5 (Fig. 1B) and EM measurements of mitochondrial morphologies, autophagosomes, axonal damage, myelin loss and remyelination at DPI 16 (Fig. 4A-H).

3. Results

3.1. Clinical scores and demyelination are markedly elevated and remyelination is blocked in EAE/Thy1-MCU Def mice relative to EAE/Thy1 controls

Female Thy1 and Thy1-MCU Def mice (15 weeks old) were subjected to EAE and clinically scored daily (DPI 7–30) (Fiander et al., 2017). Relative to the clinical scores for EAE/Thy1 controls, EAE/Thy1-MCU Def mice showed a 2-day earlier disease onset and markedly elevated disease severity from DPI 12–30 (Fig. 1A). The numbers of days at CS ≥ 1.5 was also higher for EAE/Thy1-MCU Def than EAE/Thy1 mice (Fig. 1B). ER staining revealed greater myelin loss in the spinal cords of EAE/Thy1-MCU Def than EAE/Thy1 mice at DPI 30 (Fig. 1C and D). By contrast, EAE/Thy1 and EAE/Thy1-MCU Def mice

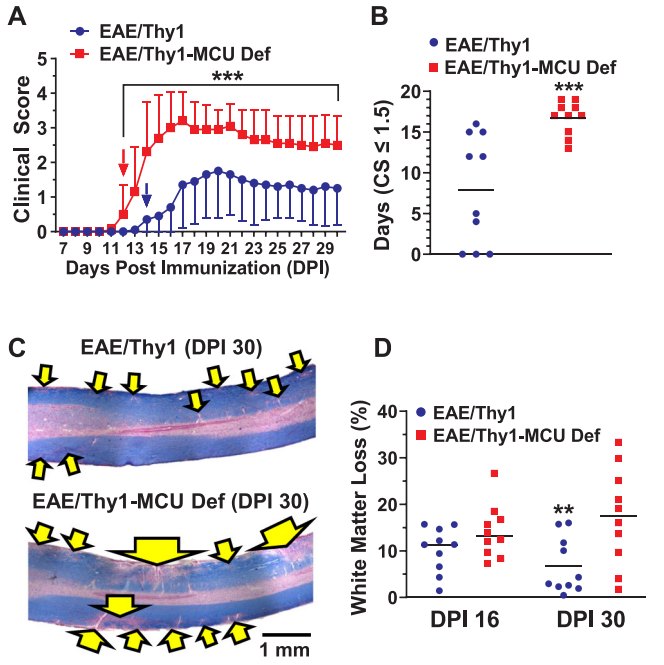

Fig. 1. Clinical scores in adult female C57Bl/6 Thy1 and Thy1-MCU deficient (Def) mice subjected to EAE (A). Each point represents the mean ± SD (n = 10/group). ***p < 0.001, two-way ANOVA. Number of days at CS ≥ 1.5 for each of these animals (B). ***p < 0.001, Mann-Whitney U test. Eriochrome cyanine staining showing myelin loss in representative longitudinal spinal cord sections of EAE/Thy1 and EAE/Thy1-MCU Def mice at DPI 30 (C). Quantification of white matter loss at DPI 16 and 30 (D). **p < 0.01 relative to all other groups, one-way ANOVA followed by Tukey's multiple comparisons test.

showed equivalent demyelination at DPI 16 (Fig. 1D). This suggests that remyelination by DPI 30 was reduced in EAE/Thy1-MCU Def mice.

3.2. Increased calpain activity and suppressed ATP concentrations in the spinal cord accompany enhanced axonal injury in EAE/Thy1-MCU Def mice

To determine if increased axon injury contributed to remyelination failure in EAE/Thy1-MCU Def mice, we quantified eYFP labelling in corticospinal axons. In CFA/Thy1 mice that do not develop EAE, diffuse eYFP labelling was evident in corticospinal axons (Fig. 2A). Axonal transection in EAE/Thy1 mice resulted in punctate eYFP labeling (Fig. 2C). This feature of axon injury was substantially increased in EAE/Thy1-MCU Def mice (Fig. 2D). Quantification of eYFP labelling revealed a 3-fold elevation of corticospinal axon injury in EAE/Thy1-MCU Def relative to EAE/Thy1 mice at both DPI 16 and 30 (Fig. 2B). Axonal injury in EAE/Thy1-MCU Def mice, but not EAE/Thy1 controls, increased from DPI 16 to DPI 30 (Fig. 2B). This was preceded at DPI 16 by a 3.0-fold elevation of calpain-cleaved αII spectrin levels and fluorometric values for calpain activity in EAE/Thy1-MCU Def relative to EAE/Thy1 mice (Fig. 2F and G). In keeping with axonal metabolic collapse at peak EAE disease severity (Kurnellas et al., 2005; Sadeghian et al., 2016), spinal cord ATP concentrations were 90% lower in EAE/Thy1 than CFA/Thy1 mice (Fig. 2H). ATP levels declined even further in EAE/Thy1-MCU Def mice to only 15% of those detected in EAE/Thy1 mice (Fig. 2H).

3.3. EAE/Thy1-MCU Def mice show morphological features of mitochondrial dysfunction and excessive autophagy in myelinated L5 spinal cord axons

To examine the effects of Thy1-MCU Def on mitochondrial function, EM was used to visualize these organelles in myelinated L5 spinal cord axons of EAE/Thy1 control and EAE/Thy1-MCU Def mice at the onset of peak disease (DPI 16). In Thy1 and Thy1-MCU Def mice not subjected to EAE (clinical score (CS) = 0), axons contained small mitochondria (diameter ~ 150 nm; Fig. 3A-D). Distinct differences in mitochondrial morphologies and cytoskeletal integrity were first seen in the myelinated axons of Thy1 and Thy1-MCU Def mice with moderate EAE (walking deficits; CS = 2.0). In EAE/Thy1 controls, the axonal cytoskeleton appeared normal while mitochondria were larger, elongated and displayed dense cristae indicative of activation (Fig. 3E and F) (Gomes and Scorrano, 2011). These changes were very rarely observed in EAE/Thy1-MCU Def mice whose axons contained far fewer activated mitochondria (Fig. 4A). Instead, EAE/Thy1-MCU Def axons contained numerous condensed and fragmented mitochondria associated with disorganized and damaged microtubules (Fig. 3G and H; Fig. 4B). Optical density measurements confirmed cytoskeletal loss in EAE/Thy1-MCU relative to EAE/Thy1 mice at CS = 2.0 (Fig. 4C). At CS = 2.5, further mitochondrial fragmentation was apparent in EAE/Thy1-MCU Def axons accompanied by the presence of large autophagosomes containing mitochondrial and cytoskeletal debris (Fig. 3K and L). By comparison, mitochondria were still activated and autophagosomes were far less common and did not appear to contain cytoskeletal debris in EAE/Thy1 axons (Fig. 3I and J; Fig. 4C). With EAE progression to CS = 3.0, numerous swollen mitochondria with damaged cristae were detected in EAE/Thy1 but not EAE/Thy1-MCU Def axons (Fig. 3M and N; Fig. 4E). At this clinical stage, autophagosomes were frequently seen digesting what appeared to be mitochondria and cytoskeletal debris in EAE/Thy1-MCU Def but not EAE/Thy1 axons (Fig. 3O and P). At CS = 3.5, massively swollen mitochondria with disintegrating cristae were observed in EAE/Thy1 axons (Fig. 3Q and R). Enhanced axonal damage in EAE/Thy1-MCU Def mice at CS = 3.5 (Fig. 4F) was characterized by the presences of numerous late (condensed) autophagosomes (Fig. 3Q-T).

3.4. Differences in mitochondrial content and morphologies in the demyelinated and remyelinating axons of EAE/Thy1 and EAE/Thy1-MCU Def mice

Examination of L5 spinal cord axons of EAE/Thy1 and EAE/Thy1-MCU Def mice with severe EAE (CS = 3.5) at DPI 16 also suggested that mitochondrial dysfunction and excessive autophagy impaired the remyelination of EAE/Thy1-MCU Def axons. At CS = 3.5, the number of remyelinating axons was 75% lower in EAE/Thy1-MCU Def mice than EAE/Thy1 controls (Fig. 4G; Fig. 5A-D). Furthermore, the number of intact mitochondria was reduced in the remyelinating axons of EAE/Thy1-MCU Def relative to EAE/Thy1 mice (Fig. 4H; Fig. 5A-D). Damaged mitochondria were also observed more frequently in the remyelinating axons of EAE/Thy1-MCU Def than EAE/Thy1 mice (Fig. 5E-H). Unlike remyelinating EAE/Thy1 axons, remyelinating EAE/Thy1-MCU Def axons typically showed signs of autophagic damage (Fig. 5E-H). In demyelinated EAE/Thy1 axons, two or more activated mitochondria were usually present (Fig. 5I, J, M and N). By contrast, demyelinated EAE/Thy1-MCU Def axons either lacked mitochondria or contained a single activated or damaged mitochondrion (Fig. 5K and L). In some damaged EAE/Thy1-MCU Def axons, a single massively swollen mitochondrion with intact outer and inner mitochondrial membranes could be seen (Fig. 5O and P).

3.5. Mitochondrial gene expression is suppressed in EAE/Thy1-MCU Def mice

To further examine the effects of Thy1-MCU Def on mitochondrial function in the EAE model, we examined mRNA levels for succinate dehydrogenase (SDH), cytochrome oxidase subunit 4 (mt-CO4) and peroxisome proliferator-activated receptor gamma coactivator 1 alpha (PGC-1α) in the spinal cords of CFA/Thy1, EAE/Thy1, CFA/Thy1-MCU Def and EAE/Thy1-MCU Def mice at DPI 16. SDH, mt-CO4 and PGC-1α

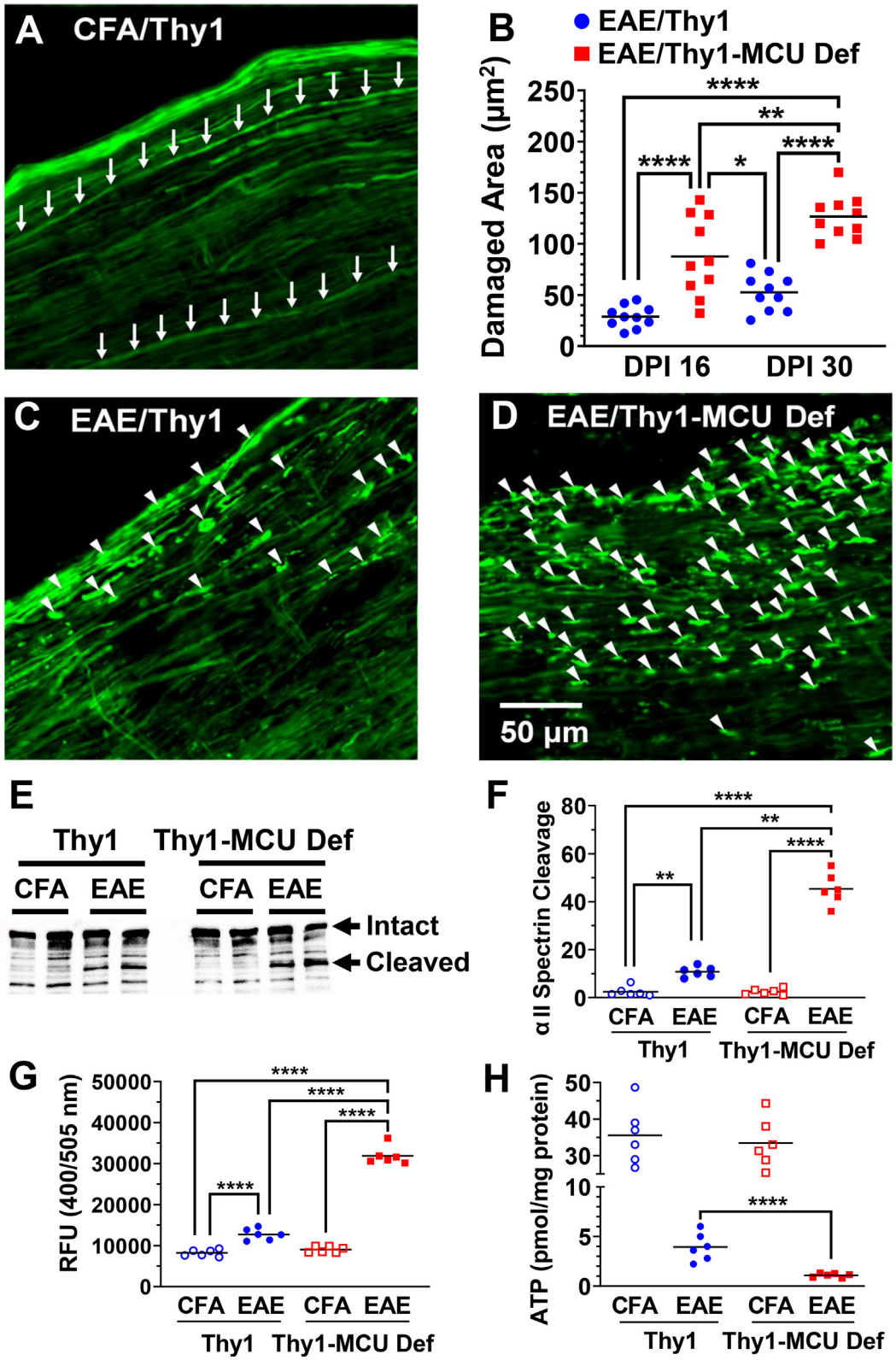

Fig. 2. Images of eYFP fluorescence in corticospinal axons at L5 of representative MOG35–55-immunization adult female control Thy1 (CFA/Thy1) (A), EAE/Thy1 (C) and EAE/Thy1-MCU Def mice at DPI 30 (D). Axon damage was assessed at DPI 16 and DPI 30 by quantifying the area occupied by eYFP labelling (B). Western blot showing calpain-cleaved αII-spectrin in the spinal cord (E). Quantification of calpain-cleaved αII-spectrin normalized to intact αII-spectrin in total protein extracts of the spinal cord at DPI 16 (F). Relative fluorescence units (RFU) in a fluorometric calpain cleavage assay (G). substrate recognition subunit ATP concentrations in the spinal cord at DPI 16 (H). *$p < 0.05$, **$p < 0.01$, ****$p < 0.0001$, one-way ANOVA followed by Tukey's multiple comparisons test.

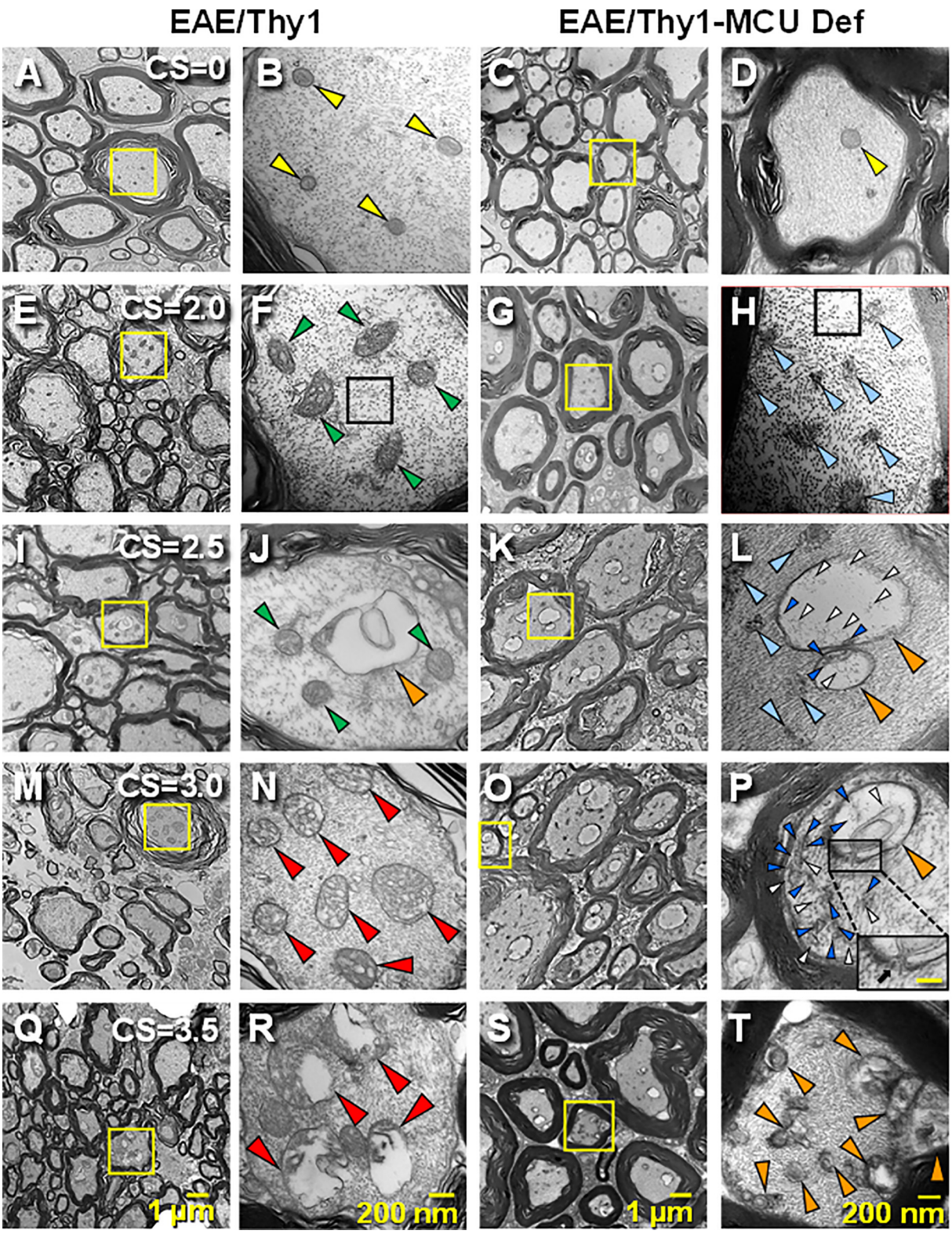

Fig. 3. Representative spinal cord (L5) EM images of EAE/Thy1 and EAE/Thy1-MCU Def mice with increasing clinical scores (CS = 0, A-D; CS = 2.0, *E*-H; CS = 2.5, I-L; CS = 3.0, M-P; CS = 3.5, Q-T) at DPI 16. Boxes: yellow (A, C, E, G, I, K, M, O, Q and S) indicate regions shown in the adjacent images (B, D, F, H, J, L, N, P, R and T) and black (panels F and H) show areas quantified for cytoskeletal optical density. Arrowheads: yellow (C and D), green (F and J), light blue (H and L) and large red (N and R) - normal, activated, fragmented and swollen mitochondria, respectively; large orange (J, L and P) - autophagosome; small blue (L and P) - mitochondrial fragments; small white (L and P) -cytoskeletal fragments; small orange (T) - condensed (late) autophagosome. Small black rectangle (P) shows an active autophagosome. Black rectangle (P) show an enlarged view of an autophagosome (bar = 350 nm). The black arrow indicates cytoskeletal fragments entering the mouth of an autophagosome. (For interpretation of the references to colour in this figure legend, the reader is referred to the web version of this article.)

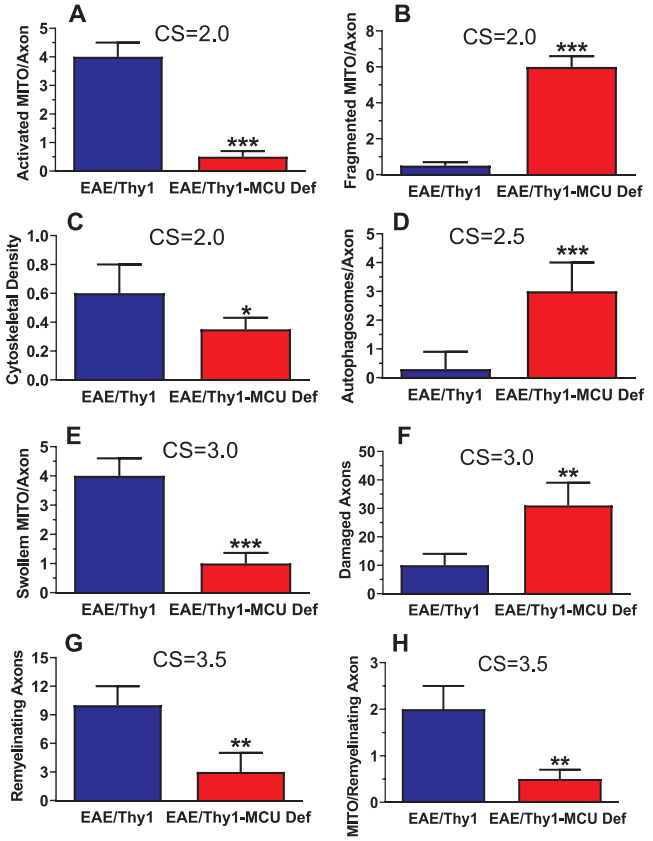

Fig. 4. Quantification of activated mitochondria (MITO; A), condensed and fragmented MITO, (B) cytoskeletal density (C), autophagosomes (D), swollen MITO/axon (E), damaged axons (F), remyelinating axons (G) and MITO/re-myelinated axon (H) in EAE/Thy1 and EAE/Thy1-MCU Def mice at CS = 2.0–3.5. Bars represent the mean ± SD (n = 4/group) **p < 0.01 and ***p < 0.001, Mann-Whitney U tests.

mRNA levels were reduced in EAE/Thy1-MCU Def relative to CFA/Thy1, CFA/Thy1-MCU Def mice and EAE/Thy1 mice (Supp. Fig. 1A-C).

3.6. Autophagy-related (atg) gene mRNAs and LC3 immunolabeling of Thy1-expressing neurons are elevated in EAE/Thy1-MCU Def mice

In view of morphological evidence of excessive autophagy in the axons of EAE/Thy1-MCU Def mice, we compared atg5 and atg7 mRNA levels in the spinal cords of CFA/Thy1,EAE/Thy1, CFA/Thy1-MCU Def and EAE/Thy1-MCU Def mice. Relative to CFA/Thy1, EAE/Thy1 and CFA/Thy1-MCU Def mice, atg5 and atg7 mRNA levels were elevated in EAE/Thy1-MCU Def mice at the onset of peak disease (DPI 16; Fig. 6A and B). Immunolabeling with LC3 revealed that this autophagosome marker was found far more frequently in the Thy1-expressing spinal cord neurons of EAE/Thy1-MCU Def than EAE/Thy1 mice (Fig. 6C-I).

3.7. Elevated immune cell activation and infiltration in EAE/Thy1-MCU Def mice

Flow cytometry was employed to compare T lymphocyte and myeloid cell populations in.

the spleens and CNS (brain and spinal cord) of CFA/Thy1, EAE/Thy1,CFA/Thy1-MCU Def and EAE/Thy1-MCU Def mice at DPI 16. Western blotting confirmed that MCU levels were reduced in the spinal cords but not the splenocytes of Thy1-MCU Def relative to Thy1 mice (Fig. 7A and B). $CD4^+$ and $CD8^+$ T cell populations were significantly increased in the spleen of EAE/Thy1-MCU Def compared to CFA/Thy1, CFA/Thy1-MCU Def and EAE/Thy1 mice (Fig. 7C). $CD4^+$ and $CD8^+$ T infiltration in the CNS were elevated in both EAE/Thy1 and EAE/Thy1-MCU Def mice relative to their CFA controls (Fig. 7D). By comparison, $CD4^+$ and $CD8^+$T cells were more prevalent in the CNS of EAE/Thy1-MCU Def compared to EAE/Thy1 mice. The percentages of $Ly6C_{low}$ and $Ly6C_{high}$ myeloid cells in the spleen were similar for all four groups (Fig. 7E). Increased CNS immune cell infiltration in EAE/Thy1-MCU Def mice was also characterized by higher $Ly6C_{low}$ and $Ly6C_{high}$ myeloid CNS cell percentages than EAE/Thy1 mice. $Ly6C_{high}$ cells, known to become pro-inflammatory macrophages and dendritic cells, were also elevated in the CNS of EAE/Thy1-MCU Def mice relative to their EAE/Thy1 controls (Fig. 7F).

3.8. Cytokine mRNA levels reflect increased pro-inflammatory and blunted pro-repair responses in the spinal cords of EAE/Thy1-MCU Def mice

Lastly, we compared mRNA levels for pro-inflammatory [interferon-γ (IFN-γ), tumour necrosis factor-α (TNF-α), interleukin-1 (IL-1β), IL-6, IL-12 (p35) and chemokine (C−C motif) ligand 5 (CCL-5)] and pro-repair [transforming growth factor-β (TGF-β) and IL-10] cytokines in the spinal cords of CFA/Thy1, EAE/Thy1, CFA/Thy1-MCU Def and EAE/Thy1-MCU Def mice at DPI 16. Relative to the CFA/Thy1 controls, IFN-γ, IL-1β, TNF-α, IL-6, IL-12 (p35) and CCL-5 mRNA levels were elevated in EAE/Thy1 mice (Fig. 8A-F). By comparison to EAE/Thy1 mice, mRNA levels for these pro-inflammatory cytokines were all higher in EAE/Thy1-MCU Def mice. Pro-repair cytokine (TGF-β and IL-10) mRNA levels were increased in EAE/Thy1 relative to CFA/Thy1 mice at the onset of remyelination (Fig. 8G and H). TGF-β and IL-10 were also elevated in EAE/Thy1-MCU Def compared to their CFA controls. However, TGF-β and IL-10 mRNA levels were similar in EAE/Thy1 and EAE/Thy1-MCU Def mice. Hence, relative to pro-inflammatory cytokines mRNA levels, there was not a proportional increase of pro-repair cytokines in EAE/Thy1-MCU Def mice.

4. Discussion

4.1. MCU activity compensates for the metabolic stress imposed by EAE on spinal cord axons

Based on evidence that enhanced MCU-mediated Ca^{2+} uptake triggers mitochondrial undocking, increases Ca^{2+} buffering and stimulates ATP synthesis (Baughman et al., 2011; Chang et al., 2011; De et al., 2011; Glancy and Balaban, 2012; Hansford and Zorov, 1998; Pan et al., 2013; Schwarz, 2013), we have proposed that the MCU plays a pivotal role in the survival of axons exposed to autoimmune-mediated demyelination. Our first series of experiments support this hypothesis by showing that disease severity, spinal cord demyelination and corticospinal axon injury were markedly elevated in EAE/Thy1-MCU Def relative to EAE/Thy1 mice at DPI 16 and 30. Furthermore, EAE/Thy1-MCU Def mice suffered more days at CS ≥ 1.5 and increased axonal injury from DPI 16 to DPI 30. These findings suggest that axonal injury blocked clinical recovery and remyelination in EAE/Thy1-MCU Def mice. Indeed, extensive injury was often seen in the absence of myelin loss in the EM images of EAE/Thy1-MCU Def spinal axons. Our findings suggest that suppressed mitochondrial-mediated Ca^{2+} buffering and ATP production contributed to increased axonal damage in these mice. With respect to the former mechanism, calpain activity was elevated by 3-fold in the spinal cords of EAE/Thy1-MCU Def compared to EAE/Thy1 mice at DPI 16. This suggests that reduced Ca^{2+} buffering in EAE/Thy1-MCU Def axons promoted injury by excessively activating this Ca^{2+}-dependent protease. Biochemical and histochemical studies have shown that CNS axon damage in EAE and MS are associated with Ca^{2+}-dependent phospholipase and calpain inductions (Diaz-Sanchez et al., 2006; Guyton et al., 2005; Kalyvas et al., 2009; Shields et al., 1999). Furthermore, oral administration of the calpain inhibitor SNJ-1945 improves axon loss and motor deficits in EAE mice (Trager et al., 2014). Hence, it seems likely that calpain-induced axonal injury played a role

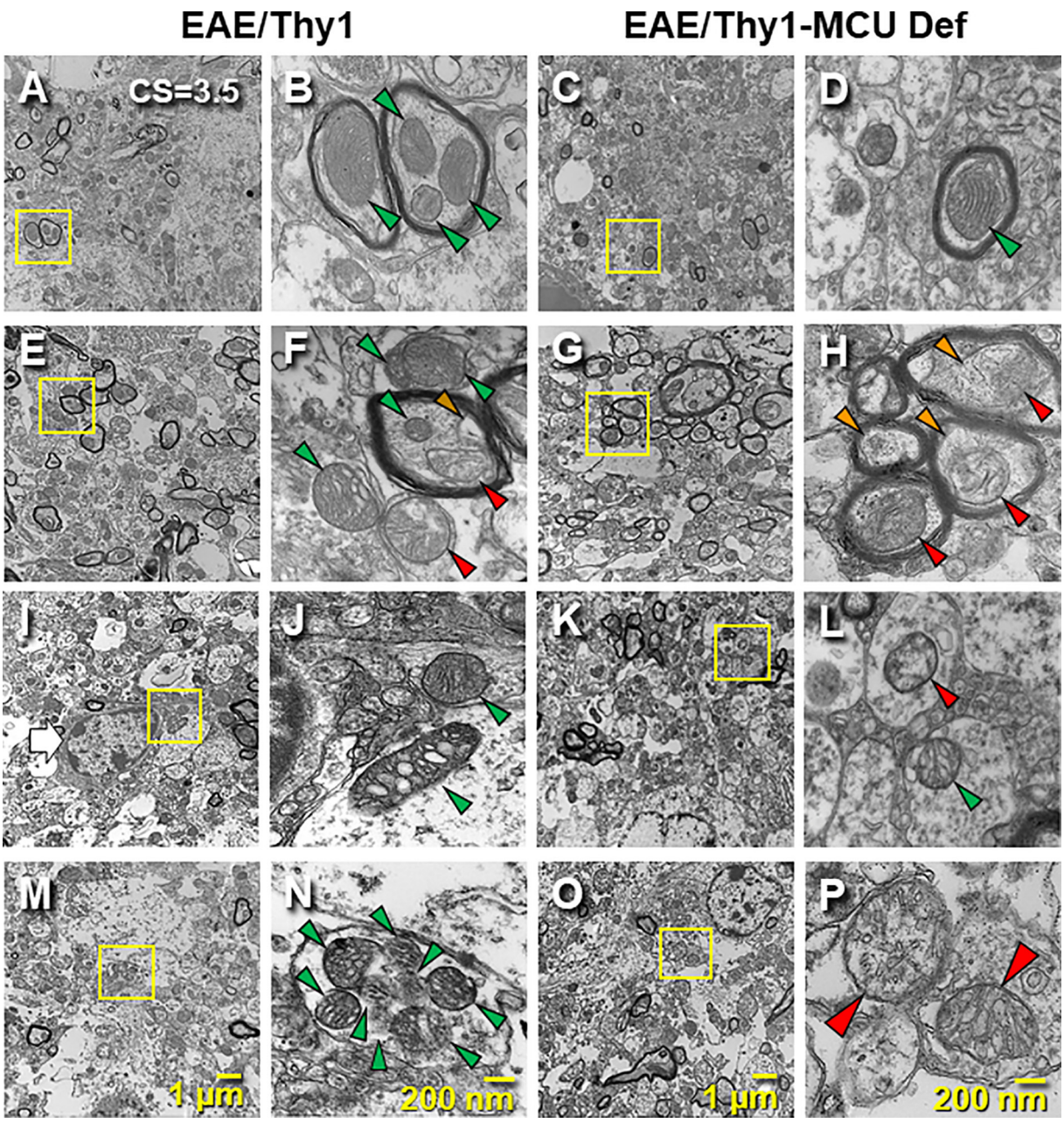

Fig. 5. Representative spinal cord (L3–5) EM images of EAE/Thy1 and EAE/Thy1-MCU Def mice with comparable clinical scores (CS = 3.5). Boxes: yellow (A, C, E, G, I, K, M, and O) indicate regions shown in the adjacent images (B, D, F, H, J, L, N and P). Arrowheads: green (B, D, F, J, L and N) and red (F, H, L and P) - activated and damaged mitochondria, respectively; brown (F) - mitophagosome; large red (P) - massively swollen but intact mitochondria; orange (H) - autophagosome. Remyelinating (A-H) and demyelinated axons (I-L) in EAE/Thy1 and EAE/Thy1-MCU Def mice. (For interpretation of the references to colour in this figure legend, the reader is referred to the web version of this article.)

in disrupting remyelination in the spinal cords of EAE/Thy1-MCU Def mice.

4.2. Suppressed ATP synthesis, mitochondrial gene expression and remyelination in EAE/Thy1-MCU Def mice

In keeping with a massive depolarization of the Ψ_m in the spinal cord axons of EAE mice at peak disease (Sadeghian et al., 2016), we observed a 90% reduction of ATP concentrations in spinal cord extracts from EAE/Thy1 mice at DPI 16. Thy1-MCU Def produced a further 85% reduction in ATP concentrations. Indeed, we have recently shown that the cell permeable MCU inhibitor Ru265 suppresses mitochondrial respiration and reduces viability in cortical neuron cultures (Novorolsky et al., 2020). Reduced ATP levels were accompanied by decreased mRNA levels for SDH, mt-CO4 and PGC-1α in EAE/Thy1-MCU Def relative to EAE/Thy1 mice. These findings are consistent with impaired CNS mitochondrial function and biogenesis in MS (Campbell and Mahad, 2012; Dutta et al., 2006; Witte et al., 2014; Witte et al., 2013). Mitochondrial dysfunction appeared to have catastrophic metabolic consequences for EAE/Thy1-MCU Def axons under immune-mediated attack as suggested by mitochondrial fragmentation, cytoskeletal integrity loss and increased autophagosome formation.

4.3. Distinct axon injury mechanisms in EAE/Thy1 and EAE/Thy1-MCU Def mice

To better understand how Thy1-MCU Def promoted axonal loss in the EAE model, EM was employed to examine the morphological

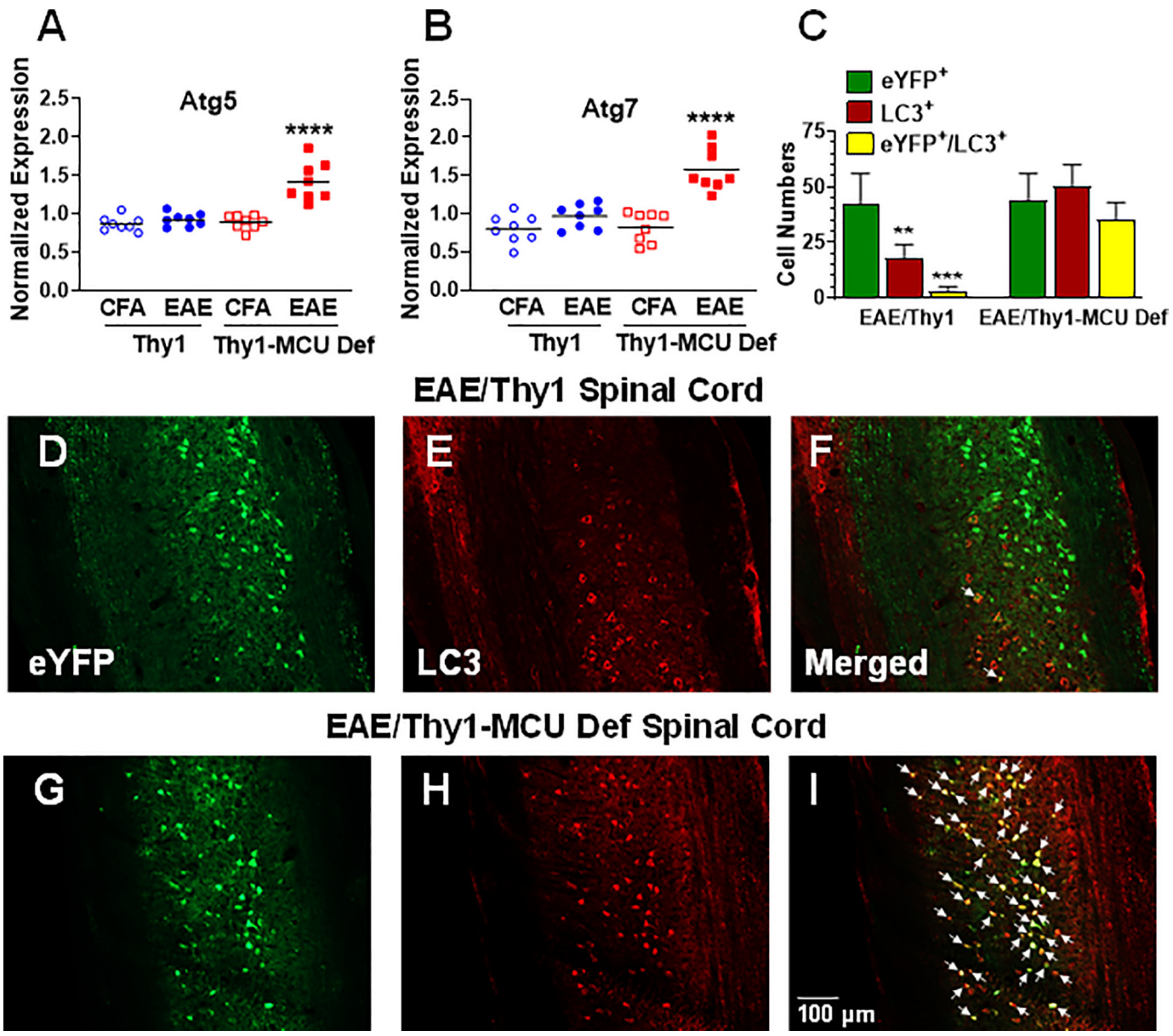

Fig. 6. Atg5 and Atg7 mRNA levels in total RNA extracts from the spinal cords of Thy1 and Thy1-MCU deficient (Thy1-MCU Def) mice 16 days after injections of just CFA and pertussis toxin (MOG35–55 immunization controls, CFA) or CFA + pertussis toxin + MOG35–55 (EAE) determined by qRT-PCR (A and B). ****$p < 0.001$, relative to all other groups, one-way ANOVA followed by Tukey's multiple comparison tests. Quantification of eYFP, LC3 and eYFP/LC3 positive neurons in the spinal cords of EAE/Thy1 and EAE/Thy1-MCU Def mice (C). Representative images of eYFP (green), LC3 (red) and eYFP/LC3 (yellow) positive spinal cord neurons in EAE/Thy1 and EAE/Thy1-MCU Def mice. Bars represent the mean ± SD ($n = 5$/group) (D-I). **$p < 0.01$ and ***$p < 0.001$ relative to EAE/Thy1-MCU Def mice, one-way ANOVA followed by Tukey's multiple comparisons test. (For interpretation of the references to colour in this figure legend, the reader is referred to the web version of this article.)

features of L5 spinal cord axons in EAE/Thy1 and EAE/Thy1-MCU Def mice with different EAE severities. Our studies revealed that axonal mitochondria in these two groups of mice responded differently to autoimmune-mediated demyelination. At the onset of walking deficits in EAE/Thy1 mice (CS = 2.0), axonal mitochondria appeared larger, elongated in shape, and displayed dense cristae suggestive of an activated state (Gomes et al., 2011; Gomes et al., 2011). By stark contrast, mitochondria in EAE/Thy1-MCU Def mice were fragmented and surrounded by clusters of disorganized microtubules. Densitometric measurements verified cytoskeletal loss in EAE/Thy1-MCU Def axons. With increased disease severity (CS = 2.5), large autophagosomes were more common in the axons of EAE/Thy1-MCU Def than EAE/Thy1 mice. Furthermore, these autophagosomes became more numerous with EAE progression. Mitochondrial and cytoskeletal debris were also evident in the autophagosomes of EAE/Thy1-MCU Def mice. It is tempting to speculate that failed mitochondrial undocking, caused by impaired MCU-mediated Ca^{2+} uptake, resulted in the collateral cytoskeletal damage in EAE/Thy1-MCU Def mice. As disease severity increased to CS = 3.0, clear signs of mitophagy were apparent in the axonal mitochondria of EAE/Thy1 mice. This was characterized by mitochondrial swelling and loss of cristae integrity in EAE/Thy1 axons that became more pronounced at CS = 3.5. These findings suggest that mitochondria in EAE/Thy1 axons undergo mitophagy whereas mitochondrial collapse in EAE/Thy1-MCU Def axons triggered excessive autophagy.

4.4. EAE/Thy1-MCU Def mice model excessive autophagy induction in MS

Autophagy acts primarily as a cell survival mechanism during

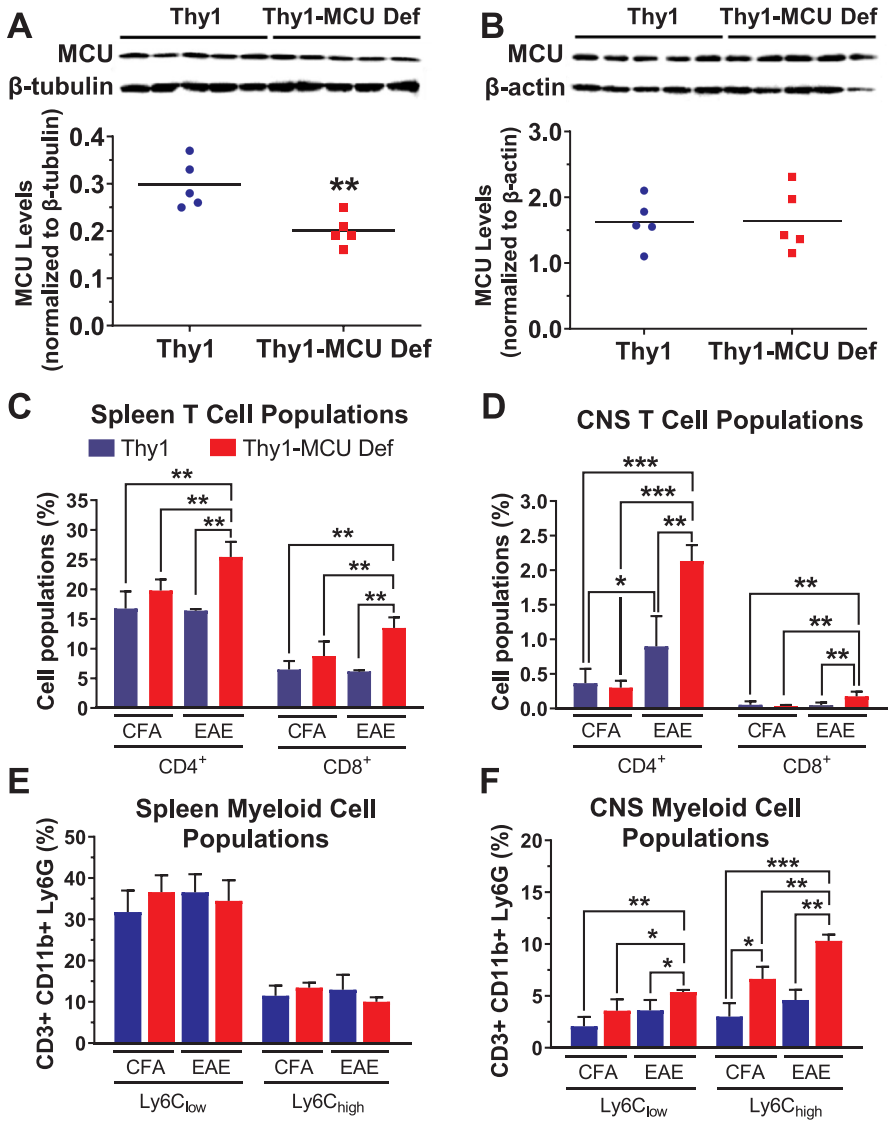

Fig. 7. Western blotting and quantification of protein extracts isolated from the spinal cords (A) and splenocytes (B) of adult female Thy1 and Thy1-MCU Def mice. Cytometric analysis of $CD4^+$ and $CD8^+$ T lymphocyte (C and D) and $Ly6C_{low}$ and $Ly6C_{high}$ myeloid cell (E and F) populations in the spleen (C and E) and CNS (brain and spinal cord; D and F) of Thy1 and Thy1-MCU Def mice 16 days after injections of just CFA and pertussis toxin ($MOG_{35–55}$ immunization controls, CFA) or CFA + MOG35–55 and pertussis toxin (EAE). Bars show mean ± SD (n = 5/group). *p < 0.05, **p < 0.01 and ***p < 0.001, one-way ANOVA followed by Tukey's multiple comparisons test.

nutrient starvation. However, in certain pathological states it also induces cell death by excessively degrading cellular contents (Fuchs and Steller, 2011; Marino et al., 2014). We have previously shown that the expression of atg5 in the CNS is strongly correlated with MS disease severity (Alirezaei et al., 2009). The ability of autophagy inhibitors to reduce paralysis and spinal cord damage in EAE mice further suggests a pathological role for autophagy in MS (Bhattacharya et al., 2014; Li et al., 2019). Mitochondria that elongate and generate more cristae in response to increased energy demands are spared from autophagy (Gomes et al., 2011). These morphological adaptations were absent in EAE/Thy1-MCU Def mice. Instead, EAE/Thy1-MCU Def axons were riddled with autophagosomes. The higher levels of atg5 and atg7 mRNAs and co-localization of LC3 in Thy1-expressing spinal neurons of EAE/Thy1-MCU Def than EAE/Thy1 mice are also indicative of autophagy induction. These findings are consistent with *in vitro* evidence of autophagy induction by suppressed MCU activity (Cardenas et al., 2010; Kondratskyi et al., 2018; Mallilankaraman et al., 2012). Lastly, the injurious effects of excessive autophagy are suggested by increased damaged axons, reduced remyelinating axons and decreased numbers of intact mitochondria within the remyelinating axons of EAE/Thy1-MCU Def than EAE/Thy1 mice.

4.5. Patterns of immune cell infiltration and cytokine expression in EAE/Thy1-MCU Def mice reflect a pro-inflammatory bias that promotes axon damage

Flow cytometry measurements indicated that T lymphocyte ($CD4^+$ and $CD8^+$) and myeloid cell ($Ly6C_{low}$ and $Ly6C_{high}$) infiltration were elevated in the CNS of EAE/Thy1-MCU Def relative to EAE/Thy1 mice. These infiltrates were composed primarily of $CD4^+$ T cells and $Ly6C_{high}$ myeloid cells. $CD4^+$ T cells produce IFN-γ and TNF-α which mobilize the innate immune system resulting in inflammatory spinal cord damage (Corsini et al., 1996; Dendrou et al., 2015; Olsson, 1995; Olsson et al., 1990). $Ly6C_{high}$ monocytes up-regulate pro-inflammatory molecules and differentiate into dendritic cells and M1 macrophages that promote CNS damage in the EAE model (Katsumoto et al., 2014; King et al., 2009; Shechter et al., 2013). These actions are supported by higher mRNA levels for pro-inflammatory cytokines (IFN-γ, IL-1β, IL-6, IL-12 (p35) and CCL5) produced by encephalitogenic T lymphocytes, dendritic cells, neutrophils and M1 macrophages in the spinal cords of EAE/Thy1-MCU Def than EAE/Thy1 mice (Arango and Descoteaux, 2014; Domingues et al., 2010; Maimone et al., 1993). Finally, similar $Ly6C_{low}$ and $Ly6C_{high}$ numbers in the spleen of EAE/Thy1-MCU Def and EAE/Thy1 mice suggest that increased myelin and axonal damage contributed to the recruitment of these cells to the CNS of EAE/Thy1-

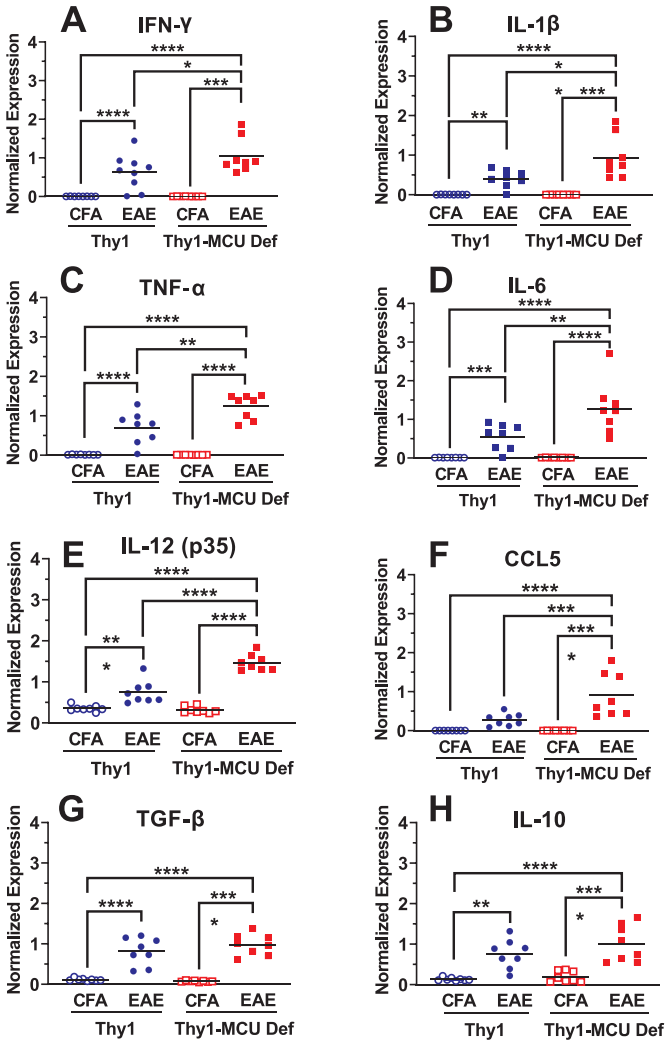

Fig. 8. Cytokine (IFNγ, IL-1β, TNFα, IL-6, IL-12 (p35), TGF-β and IL-10; A-E, G and H) and chemokine (CCL-5; F) mRNA levels in total RNA extracts from the spinal cords of adult female Thy1 and Thy1-MCU deficient (Thy1-MCU Def) mice 16 days after injections of just CFA and pertussis toxin ($MOG_{35–55}$ immunization controls, CFA) or CFA + pertussis toxin + $MOG_{35–55}$ (EAE) determined by qRT-PCR (A-H). *p < 0.05, **p < 0.01, ***p < 0.001 and ****p < 0.0001, one-way ANOVA followed by Tukey's multiple comparisons test.

MCU Def mice.

5. Limitations of conclusions based on correlative data

Our findings suggest that mitochondrial dysfunction suppressed Ca^{2+} buffering, ATP synthesis and mitochondrial gene expression resulting in the metabolic collapse of EAE/Thy1-MCU Def axons at DPI 16 which was characterized by excessive autophagy and increased inflammation relative to the EAE/Thy1 controls. Based on these findings and the further elevation of axonal injury in EAE/Thy1-MCU Def mice at DPI 30, we have proposed that axonal injury blocked remyelination in these animals at DPI 30. However, we acknowledge that causality is not proven by these by correlations.

6. Futures studies

The flavonoids quercetin and kaempferol have been shown to increase MCU activity in HeLa cells and human fibroblasts (Montero et al., 2004; Vay et al., 2007). We have previously reported that quercetin enhances mitochondrial respiration and protects primary cultures of mouse cortical neurons from viability loss by a lethal period of oxygen glucose deprivation (Nichols et al., 2015). Furthermore, we have shown that oral administration of flavonoid-rich extract AF4 which contains high amounts of quercetin and kaempferol reduces disease severity and spinal cord damage in EAE mice (Warford et al., 2014). Comparisons of disease severity and axonal injury in EAE/Thy1 and EAE/Thy1-MCU Def mice treated with quercetin or kaempferol would establish the contribution of MCU activation in spinal cord neurons to the beneficial effects of these compounds.

7. Conclusions

These findings indicate that EAE/Thy1-MCU Def axons model "inside-out" mechanisms proposed for the propagation of neuroinflammation in MS (Chrzanowski et al., 2019; Milo et al., 2019; Scheld et al., 2016). We propose that drug screening efforts based on the reversal of these MCU-dependent metabolic deficits in cultured neurons may rapidly identify novel neuroprotective and remyelinating agents for progressive MS. Testing of these therapeutic candidates in EAE/Thy1-MCU mice may thus offer a novel approach to prioritize them for clinical development.

Supplementary data to this article can be found online at https://doi.org/10.1016/j.expneurol.2020.113430.

Funding

This work was funded by a biomedical research grant from the MS Society of Canada (EGID 2983; GSR). We gratefully acknowledge Aruloli Thirumaran for excellent technical assistance.

Declaration of Competing Interest

The author(s) declared no potential conflicts of interest with respect to the research, authorship, and/or publication of this article.

Authors' contributions

SPH, AL, MDJF, MN and RJN assisted with the EAE studies, histology, statistical analysis and preparation of the manuscript. BEK, PK and SG performed the flow cytometry and statistical analysis of the resultant data and assisted with the preparation of the manuscript. GSR assisted with the statistical analysis and preparation of the manuscript.

References

Alirezaei, M., Fox, H.S., Flynn, C.T., Moore, C.S., Hebb, A.L., Frausto, R.F., Bhan, V., Kiosses, W.B., Whitton, J.L., Robertson, G.S., Crocker, S.J., 2009. Elevated ATG5 expression in autoimmune demyelination and multiple sclerosis. Autophagy. 5, 152–158.

Arango, D.G., Descoteaux, A., 2014. Macrophage cytokines: involvement in immunity and infectious diseases. Front. Immunol. 5, 491.

Baughman, J.M., Perocchi, F., Girgis, H.S., Plovanich, M., Belcher-Timme, C.A., Sancak, Y., Bao, X.R., Strittmatter, L., Goldberger, O., Bogorad, R.L., Koteliansky, V., Mootha, V.K., 2011. Integrative genomics identifies MCU as an essential component of the mitochondrial calcium uniporter. Nature 476, 341–345.

Bhattacharya, A., Parillon, X., Zeng, S., Han, S., Eissa, N.T., 2014. Deficiency of autophagy in dendritic cells protects against experimental autoimmune encephalomyelitis. J. Biol. Chem. 289, 26525–26532.

Bustin, S.A., Benes, V., Garson, J.A., Hellemans, J., Huggett, J., Kubista, M., Mueller, R., Nolan, T., Pfaffl, M.W., Shipley, G.L., Vandesompele, J., Wittwer, C.T., 2009. The MIQE guidelines: minimum information for publication of quantitative real-time PCR experiments. Clin. Chem. 55, 611–622.

Campbell, G.R., Mahad, D.J., 2012. Mitochondrial changes associated with demyelination: consequences for axonal integrity. Mitochondrion. 12, 173–179.

Campbell, G., Mahad, D., 2018. Neurodegeneration in Progressive Multiple Sclerosis. Cold Spring Harb. Perspect. Med. 8.

Cardenas, C., Miller, R.A., Smith, I., Bui, T., Molgo, J., Muller, M., Vais, H., Cheung, K.H., Yang, J., Parker, I., Thompson, C.B., Birnbaum, M.J., Hallows, K.R., Foskett, J.K., 2010. Essential regulation of cell bioenergetics by constitutive InsP3 receptor Ca2+ transfer to mitochondria. Cell 142, 270–283.

Chang, K.T., Niescier, R.F., Min, K.T., 2011. Mitochondrial matrix Ca2+ as an intrinsic signal regulating mitochondrial motility in axons. Proc. Natl. Acad. Sci. U. S. A. 108, 15456–15461.

Charcot, J.M., 1868. Histologie de la sclerose en plaque. In: Gaz Hop Civils Militaires. 44. pp. 554–566.
Chrzanowski, U., Bhattarai, S., Scheld, M., Clarner, T., Fallier-Becker, P., Beyer, C., Rohr, S.O., Schmitz, C., Hochstrasser, T., Schweiger, F., Amor, S., Horn-Bochtler, A., Denecke, B., Nyamoya, S., Kipp, M., 2019. Oligodendrocyte degeneration and concomitant microglia activation directs peripheral immune cells into the forebrain. Neurochem. Int. 126, 139–153.
Compston, A., Coles, A., 2008. Multiple sclerosis. Lancet 372, 1502–1517.
Corsini, E., Dufour, A., Ciusani, E., Gelati, M., Frigerio, S., Gritti, A., Cajola, L., Mancardi, G.L., Massa, G., Salmaggi, A., 1996. Human brain endothelial cells and astrocytes produce IL-1 beta but not IL-10. Scand. J. Immunol. 44, 506–511.
De, S.D., Raffaello, A., Teardo, E., Szabo, I., Rizzuto, R., 2011. A forty-kilodalton protein of the inner membrane is the mitochondrial calcium uniporter. Nature 476, 336–340.
Deluca, H.F., Engstrom, G.W., 1961. Calcium uptake by rat kidney mitochondria. Proc. Natl. Acad. Sci. U. S. A. 47, 1744–1750.
Dendrou, C.A., Fugger, L., Friese, M.A., 2015. Immunopathology of multiple sclerosis. Nat. Rev. Immunol. 15, 545–558.
Denton, R.M., Randle, P.J., Martin, B.R., 1972. Stimulation by calcium ions of pyruvate dehydrogenase phosphate phosphatase. Biochem. J. 128, 161–163.
Diaz-Sanchez, M., Williams, K., DeLuca, G.C., Esiri, M.M., 2006. Protein co-expression with axonal injury in multiple sclerosis plaques. Acta Neuropathol. 111, 289–299.
Domingues, H.S., Mues, M., Lassmann, H., Wekerle, H., Krishnamoorthy, G., 2010. Functional and pathogenic differences of Th1 and Th17 cells in experimental autoimmune encephalomyelitis. PLoS One 5, e15531.
Dutta, R., Trapp, B.D., 2012. Gene expression profiling in multiple sclerosis brain. Neurobiol. Dis. 45, 108–114.
Dutta, R., McDonough, J., Yin, X., Peterson, J., Chang, A., Torres, T., Gudz, T., Macklin, W.B., Lewis, D.A., Fox, R.J., Rudick, R., Mirnics, K., Trapp, B.D., 2006. Mitochondrial dysfunction as a cause of axonal degeneration in multiple sclerosis patients. Ann. Neurol. 59, 478–489.
Fiander, M.D., Stifani, N., Nichols, M., Akay, T., Robertson, G.S., 2017. Kinematic gait parameters are highly sensitive measures of motor deficits and spinal cord injury in mice subjected to experimental autoimmune encephalomyelitis. Behav. Brain Res. 317, 95–108.
Fischer, M.T., Sharma, R., Lim, J.L., Haider, L., Frischer, J.M., Drexhage, J., Mahad, D., Bradl, M., van, H.J., Lassmann, H., 2012. NADPH oxidase expression in active multiple sclerosis lesions in relation to oxidative tissue damage and mitochondrial injury. Brain 135, 886–899.
Franklin, R.J., Ffrench-Constant, C., Edgar, J.M., Smith, K.J., 2012. Neuroprotection and repair in multiple sclerosis. Nat. Rev. Neurol. 8, 624–634.
Fuchs, Y., Steller, H., 2011. Programmed cell death in animal development and disease. Cell 147, 742–758.
Glancy, B., Balaban, R.S., 2012. Role of mitochondrial Ca2+ in the regulation of cellular energetics. Biochemistry 51, 2959–2973.
Gomes, L.C., Scorrano, L., 2011. Mitochondrial elongation during autophagy: a stereotypical response to survive in difficult times. Autophagy. 7, 1251–1253.
Gomes, L.C., Di, B.G., Scorrano, L., 2011. During autophagy mitochondria elongate, are spared from degradation and sustain cell viability. Nat. Cell Biol. 13, 589–598.
Guyton, M.K., Wingrave, J.M., Yallapragada, A.V., Wilford, G.G., Sribnick, E.A., Matzelle, D.D., Tyor, W.R., Ray, S.K., Banik, N.L., 2005. Upregulation of calpain correlates with increased neurodegeneration in acute experimental auto-immune encephalomyelitis. J. Neurosci. Res. 81, 53–61.
Hahn, A., Vonck, J., Mills, D.J., Meier, T., Kuhlbrandt, W., 2018. Structure, mechanism, and regulation of the chloroplast ATP synthase. Science 360.
Hansford, R.G., Zorov, D., 1998. Role of mitochondrial calcium transport in the control of substrate oxidation. Mol. Cell. Biochem. 184, 359–369.
Kalyvas, A., Baskakis, C., Magrioti, V., Constantinou-Kokotou, V., Stephens, D., Lopez-Vales, R., Lu, J.Q., Yong, V.W., Dennis, E.A., Kokotos, G., David, S., 2009. Differing roles for members of the phospholipase A2 superfamily in experimental autoimmune encephalomyelitis. Brain 132, 1221–1235.
Kapoor, R., Ho, P.R., Campbell, N., Chang, I., Deykin, A., Forrestal, F., Lucas, N., Yu, B., Arnold, D.L., Freedman, M.S., Goldman, M.D., Hartung, H.P., Havrdova, E.K., Jeffery, D., Miller, A., Sellebjerg, F., Cadavid, D., Mikol, D., Steiner, D., 2018. Effect of natalizumab on disease progression in secondary progressive multiple sclerosis (ASCEND): a phase 3, randomised, double-blind, placebo-controlled trial with an open-label extension. Lancet Neurol. 17, 405–415.
Kappos, L., Polman, C., Pozzilli, C., Thompson, A., 1998. Placebo-controlled multicentre randomised trial of interferon beta-1b in treatment of secondary progressive multiple sclerosis. European study group on interferon beta-1b in secondary progressive MS. Lancet 352, 1491–1497.
Katsumoto, A., Lu, H., Miranda, A.S., Ransohoff, R.M., 2014. Ontogeny and functions of central nervous system macrophages. J. Immunol. 193, 2615–2621.
King, I.L., Dickendesher, T.L., Segal, B.M., 2009. Circulating Ly-6C+ myeloid precursors migrate to the CNS and play a pathogenic role during autoimmune demyelinating disease. Blood 113, 3190–3197.
Kondratskyi, A., Kondratska, K., Skryma, R., Klionsky, D.J., Prevarskaya, N., 2018. Ion channels in the regulation of autophagy. Autophagy. 14, 3–21.
Kurnellas, M.P., Nicot, A., Shull, G.E., Elkabes, S., 2005. Plasma membrane calcium ATPase deficiency causes neuronal pathology in the spinal cord: a potential mechanism for neurodegeneration in multiple sclerosis and spinal cord injury. FASEB J. 19, 298–300.
Kwong, J.Q., Lu, X., Correll, R.N., Schwanekamp, J.A., Vagnozzi, R.J., Sargent, M.A., York, A.J., Zhang, J., Bers, D.M., Molkentin, J.D., 2015. The mitochondrial calcium Uniporter selectively matches metabolic output to acute contractile stress in the heart. Cell Rep. 12, 15–22.
Lehninger, A.L., 1979. Some aspects of energy coupling by mitochondria. Adv. Exp. Med. Biol. 111, 1–16.
Li, W., Feng, J., Gao, C., Wu, M., Du, Q., Tsoi, B., Wang, Q., Yang, D., Shen, J., 2019. Nitration of Drp1 provokes mitophagy activation mediating neuronal injury in experimental autoimmune encephalomyelitis. Free Radic. Biol. Med. 143, 70–83.
Lublin, F., Miller, D.H., Freedman, M.S., Cree, B.A.C., Wolinsky, J.S., Weiner, H., Lubetzki, C., Hartung, H.P., Montalban, X., Uitdehaag, B.M.J., Merschhemke, M., Li, B., Putzki, N., Liu, F.C., Haring, D.A., Kappos, L., 2016. Oral fingolimod in primary progressive multiple sclerosis (INFORMS): a phase 3, randomised, double-blind, placebo-controlled trial. Lancet 387, 1075–1084.
Luongo, T.S., Lambert, J.P., Yuan, A., Zhang, X., Gross, P., Song, J., Shanmughapriya, S., Gao, E., Jain, M., Houser, S.R., Koch, W.J., Cheung, J.Y., Madesh, M., Elrod, J.W., 2015. The mitochondrial calcium Uniporter matches energetic supply with cardiac workload during stress and modulates permeability transition. Cell Rep. 12, 23–34.
Mahad, D.J., Ziabreva, I., Campbell, G., Lax, N., White, K., Hanson, P.S., Lassmann, H., Turnbull, D.M., 2009. Mitochondrial changes within axons in multiple sclerosis. Brain 132, 1161–1174.
Maimone, D., Reder, A.T., Gregory, S., 1993. T cell lymphokine-induced secretion of cytokines by monocytes from patients with multiple sclerosis. Cell. Immunol. 146, 96–106.
Mallilankaraman, K., Cardenas, C., Doonan, P.J., Chandramoorthy, H.C., Irrinki, K.M., Golenar, T., Csordas, G., Madireddi, P., Yang, J., Muller, M., Miller, R., Kolesar, J.E., Molgo, J., Kaufman, B., Hajnoczky, G., Foskett, J.K., Madesh, M., 2012. MCUR1 is an essential component of mitochondrial Ca2+ uptake that regulates cellular metabolism. Nat. Cell Biol. 14, 1336–1343.
Marino, G., Niso-Santano, M., Baehrecke, E.H., Kroemer, G., 2014. Self-consumption: the interplay of autophagy and apoptosis. Nat. Rev. Mol. Cell Biol. 15, 81–94.
Milo, R., Korczyn, A.D., Manouchehri, N., Stuve, O., 2019. The temporal and causal relationship between inflammation and neurodegeneration in multiple sclerosis. Mult. Scler. 1–11.
Montalban, X., Hauser, S.L., Kappos, L., Arnold, D.L., Bar-Or, A., Comi, G., De, S.J., Giovannoni, G., Hartung, H.P., Hemmer, B., Lublin, F., Rammohan, K.W., Selmaj, K., Traboulsee, A., Sauter, A., Masterman, D., Fontoura, P., Belachew, S., Garren, H., Mairon, N., Chin, P., Wolinsky, J.S., 2017. Ocrelizumab versus placebo in primary progressive multiple sclerosis. N. Engl. J. Med. 376, 209–220.
Montero, M., Lobaton, C.D., Hernandez-Sanmiguel, E., Santodomingo, J., Vay, L., Moreno, A., Alvarez, J., 2004. Direct activation of the mitochondrial calcium uniporter by natural plant flavonoids. Biochem. J. 384, 19–24.
Nichols, M., Zhang, J., Polster, B.M., Elustondo, P.A., Thirumaran, A., Pavlov, E.V., Robertson, G.S., 2015. Synergistic neuroprotection by epicatechin and quercetin: activation of convergent mitochondrial signaling pathways. Neuroscience 308, 75–94.
Nichols, M., Elustondo, P.A., Warford, J., Thirumaran, A., Pavlov, E.V., Robertson, G.S., 2017. Global ablation of the mitochondrial calcium uniporter increases glycolysis in cortical neurons subjected to energetic stressors. J. Cereb. Blood Flow Metab. 37, 3027–3041.
Nichols, M., Pavlov, E.V., Robertson, G.S., 2018. Tamoxifen-induced knockdown of the mitochondrial calcium uniporter in Thy1-expressing neurons protects mice from hypoxic/ischemic brain injury. Cell Death Dis. 9, 606.
Niescier, R.F., Chang, K.T., Min, K.T., 2013. Miro, MCU, and calcium: bridging our understanding of mitochondrial movement in axons. Front. Cell. Neurosci. 7, 148.
Niescier, R.F., Hong, K., Park, D., Min, K.T., 2018. MCU interacts with Miro1 to modulate mitochondrial functions in neurons. J. Neurosci. 38, 4666–4677.
Novorolsky, R.J., Nichols, M., Kim, J.S., Pavlov, E.V., Woods, J., Wilson, J.J., Robertson, G.S., 2020. The cell-permeable mitochondrial calcium uniporter inhibitor Ru265 preserves cortical neuron respiration after lethal oxygen glucose deprivation and reduces hypoxic/ischemic brain injury. J. Cereb. Blood Flow Metab. (6), 1172–1181.
Olsson, T., 1995. Cytokine-producing cells in experimental autoimmune encephalomyelitis and multiple sclerosis. Neurology 45, S11–S15.
Olsson, T., Zhi, W.W., Hojeberg, B., Kostulas, V., Jiang, Y.P., Anderson, G., Ekre, H.P., Link, H., 1990. Autoreactive T lymphocytes in multiple sclerosis determined by antigen-induced secretion of interferon-gamma. J. Clin. Invest. 86, 981–985.
Pan, X., Liu, J., Nguyen, T., Liu, C., Sun, J., Teng, Y., Fergusson, M.M., Rovira, I.I., Allen, M., Springer, D.A., Aponte, A.M., Gucek, M., Balaban, R.S., Murphy, E., Finkel, T., 2013. The physiological role of mitochondrial calcium revealed by mice lacking the mitochondrial calcium uniporter. Nat. Cell Biol. 15, 1464–1472.
Peruzzotti-Jametti, L., Pluchino, S., 2018. Targeting mitochondrial metabolism in neuroinflammation: towards a therapy for progressive multiple sclerosis. Trends Mol. Med. 24, 838–855.
Rizzuto, R., De, S.D., Raffaello, A., Mammucari, C., 2012. Mitochondria as sensors and regulators of calcium signalling. Nat. Rev. Mol. Cell Biol. 13, 566–578.
Rottenberg, H., Scarpa, A., 1974. Calcium uptake and membrane potential in mitochondria. Biochemistry 13, 4811–4817.
Sadeghian, M., Mastrolia, V., Rezaei, H.A., Mosley, A., Mullali, G., Schiza, D., Sajic, M., Hargreaves, I., Heales, S., Duchen, M.R., Smith, K.J., 2016. Mitochondrial dysfunction is an important cause of neurological deficits in an inflammatory model of multiple sclerosis. Sci. Rep. 6, 33249.
Saxton, W.M., Hollenbeck, P.J., 2012. The axonal transport of mitochondria. J. Cell Sci. 125, 2095–2104.
Scheld, M., Ruther, B.J., Grosse-Veldmann, R., Ohl, K., Tenbrock, K., Dreymuller, D., Fallier-Becker, P., Zendedel, A., Beyer, C., Clarner, T., Kipp, M., 2016. Neurodegeneration triggers peripheral immune cell recruitment into the forebrain. J. Neurosci. 36, 1410–1415.
Schwarz, T.L., 2013. Mitochondrial trafficking in neurons. Cold Spring Harb. Perspect. Biol. 6, 1–15.
Shechter, R., Miller, O., Yovel, G., Rosenzweig, N., London, A., Ruckh, J., Kim, K.W., Klein, E., Kalchenko, V., Bendel, P., Lira, S.A., Jung, S., Schwartz, M., 2013.

Recruitment of beneficial M2 macrophages to injured spinal cord is orchestrated by remote brain choroid plexus. Immunity. 38, 555–569.
Shields, D.C., Schaecher, K.E., Saido, T.C., Banik, N.L., 1999. A putative mechanism of demyelination in multiple sclerosis by a proteolytic enzyme, calpain. Proc. Natl. Acad. Sci. U. S. A. 96, 11486–11491.
Stirling, D.P., Stys, P.K., 2010. Mechanisms of axonal injury: internodal nanocomplexes and calcium deregulation. Trends Mol. Med. 16, 160–170.
Stys, P.K., Lopachin, R.M., 1998. Mechanisms of calcium and sodium fluxes in anoxic myelinated central nervous system axons. Neuroscience 82, 21–32.
Trager, N., Smith, A., Wallace, I.G., Azuma, M., Inoue, J., Beeson, C., Haque, A., Banik, N.L., 2014. Effects of a novel orally administered calpain inhibitor SNJ-1945 on immunomodulation and neurodegeneration in a murine model of multiple sclerosis. J. Neurochem. 130, 268–279.
Trapp, B.D., Stys, P.K., 2009. Virtual hypoxia and chronic necrosis of demyelinated axons in multiple sclerosis. Lancet Neurol. 8, 280–291.
Trapp, B.D., Peterson, J., Ransohoff, R.M., Rudick, R., Mork, S., Bo, L., 1998. Axonal transection in the lesions of multiple sclerosis. N. Engl. J. Med. 338, 278–285.
Tsutsui, S., Stys, P.K., 2013. Metabolic injury to axons and myelin. Exp. Neurol. 246, 26–34.
Vay, L., Hernandez-Sanmiguel, E., Santo-Domingo, J., Lobaton, C.D., Moreno, A., Montero, M., Alvarez, J., 2007. Modulation of Ca(2+) release and Ca(2+) oscillations in HeLa cells and fibroblasts by mitochondrial Ca(2+) uniporter stimulation. J. Physiol. 580, 39–49.
Warford, J., Jones, Q.R., Nichols, M., Sullivan, V., Rupasinghe, H.P., Robertson, G.S., 2014. The flavonoid-enriched fraction AF4 suppresses neuroinflammation and promotes restorative gene expression in a mouse model of experimental autoimmune encephalomyelitis. J. Neuroimmunol. 268, 71–83.
Witte, M.E., Nijland, P.G., Drexhage, J.A., Gerritsen, W., Geerts, D., van Het, H.B., Reijerkerk, A., de Vries, H.E., van D, V., Van, H.J., 2013. Reduced expression of PGC-1alpha partly underlies mitochondrial changes and correlates with neuronal loss in multiple sclerosis cortex. Acta Neuropathol. 125, 231–243.
Witte, M.E., Mahad, D.J., Lassmann, H., van, H.J., 2014. Mitochondrial dysfunction contributes to neurodegeneration in multiple sclerosis. Trends Mol. Med. 20, 179–187.